Dynamics of Hole Singlet-Triplet Qubits with Large g-Factor Differences

Daniel Jirovec,[1,*] Philipp M. Mutter,[2,†] Andrea Hofmann,[1,3] Alessandro Crippa,[1,4] Marek Rychetsky,[5] David L. Craig,[5] Josip Kukucka,[1] Frederico Martins,[1,6] Andrea Ballabio,[7] Natalia Ares,[8] Daniel Chrastina,[7] Giovanni Isella,[7] Guido Burkard,[2] and Georgios Katsaros[1]

[1]*Institute of Science and Technology Austria (ISTA), Am Campus 1, 3400 Klosterneuburg, Austria*
[2]*Department of Physics, University of Konstanz, D-78457 Konstanz, Germany*
[3]*Department of Physics, University of Basel, Klingelbergstrasse 82, CH-4056 Basel, Switzerland*
[4]*NEST, Istituto Nanoscienze-CNR and Scuola Normale Superiore, I-56127 Pisa, Italy*
[5]*Department of Materials, University of Oxford, Parks Road, Oxford OX1 3PH, United Kingdom*
[6]*Hitachi Cambridge Laboratory, J.J. Thomson Avenue, Cambridge CB3 0HE, United Kingdom*
[7]*L-NESS, Physics Department, Politecnico di Milano, via Anzani 42, 22100, Como, Italy*
[8]*Department of Engineering Science, University of Oxford, Parks Road, Oxford OX1 3PJ, United Kingdom*

(Received 6 October 2021; revised 24 January 2022; accepted 24 February 2022; published 24 March 2022)

The spin-orbit interaction permits to control the state of a spin qubit via electric fields. For holes it is particularly strong, allowing for fast all electrical qubit manipulation, and yet an in-depth understanding of this interaction in hole systems is missing. Here we investigate, experimentally and theoretically, the effect of the cubic Rashba spin-orbit interaction on the mixing of the spin states by studying singlet-triplet oscillations in a planar Ge hole double quantum dot. Landau-Zener sweeps at different magnetic field directions allow us to disentangle the effects of the spin-orbit induced spin-flip term from those caused by strongly site-dependent and anisotropic quantum dot g tensors. Our work, therefore, provides new insights into the hole spin-orbit interaction, necessary for optimizing future qubit experiments.

DOI: 10.1103/PhysRevLett.128.126803

The spin-orbit interaction (SOI) allows electrical manipulation of individual spins and has therefore become a key ingredient for the realization of fully electrically controlled spin qubits [1,2]. For electrons in Si it is rather weak and synthetically boosted by means of micromagnets [3,4]. For holes, on the other hand, it is an intrinsic property which allows to perform electron dipole spin resonance (EDSR) measurements [1,2,5–9]. In Ge it is particularly strong leading to Rabi frequencies beyond 100 MHz [7,10,11]. SOI for holes can be linear or cubic in the wave vector k, with nanowire qubits favoring the former type while planar qubits the latter [12–14]. The SOI is not only important for single spin but also for singlet-triplet qubits as it causes an intrinsic mixing between the heavy hole (HH) and light hole (LH) bands and thereby locally affects the g factors of the individual spins allowing to drive $S-T_0$ oscillations [15]. In combination with an extrinsic Rashba type SOI caused by the structural inversion asymmetry induced by the heterostructure, it also mixes the S and T_- states contributing therefore to a measurable avoided crossing Δ_{ST_-}.

Here, we investigate this avoided crossing for a double quantum dot (DQD) Ge hole spin system and gain insight into the interplay between SOI and the g-factor anisotropy and their consequences on qubit dynamics.

A scanning electron microscope (SEM) image of the device under consideration is depicted in Fig. 1(a) and further details can be found in Ref. [15]. A two-dimensional hole gas is embedded in a Ge/SiGe heterostructure and additional TiPd top gates confine a DQD and a charge sensor (CS). For qubit state selective read out we rely on Pauli spin blockade (PSB) combined with Ohmic reflectometry [16]. Fast detuning pulses are applied to gates LB and RB through an arbitrary waveform generator (AWG) with a pulse-rise time of $\tau_{\mathrm{rise}} \approx 2$ ns. Throughout this work we apply a small magnetic field in a plane perpendicular to the axis connecting the two dots (DQD axis), $\mathbf{B} = [B\cos(\theta), 0, B\sin(\theta)]$, where θ describes the tilt angle from the in-plane direction. We tune the DQD to a charge transition between an effective $(2,0) \leftrightarrow (1,1)$ state, with (n_L, n_R), where n_L (n_R) denotes the effective hole number in the left (right) QD [Fig. 1(c)]. The tunnel coupling between the dots is described by t_C while the energy detuning between the $S(2,0)$ and $S(1,1)$ state is parametrized by ϵ. Each QD is characterized by an out-of-plane and an in-plane g factor, $g_\perp$ and $g_\parallel$, respectively. However, the dynamics of singlet-triplet qubits is only

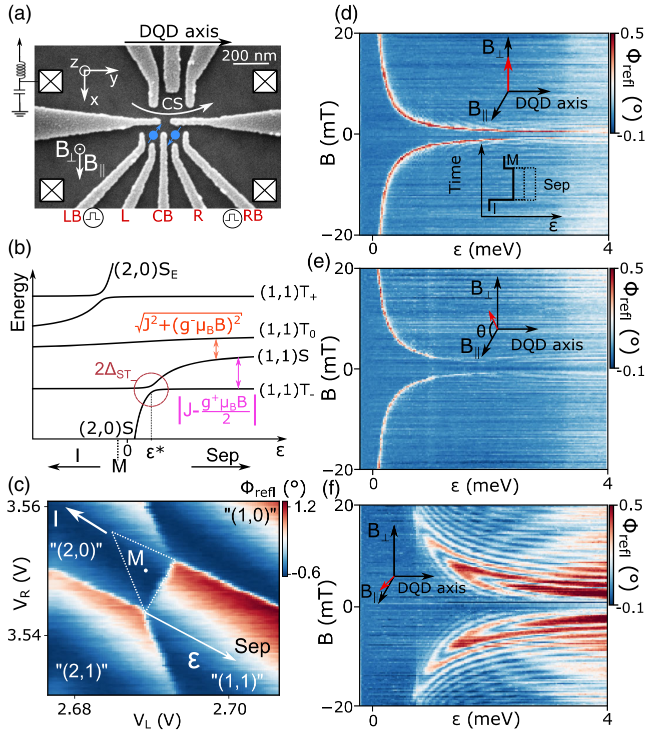

FIG. 1. (a) SEM image of the device. (b) The energy level diagram as a function of detuning highlights the relevant energy splittings between S and T_0 (orange) and S and T_- (pink). At $\epsilon = \epsilon^*$, S and T_- anticross with a splitting $2\Delta_{ST_-}$. Initialization (I) in a singlet $S(2,0)$ occurs at negative ϵ. The spins are separated (Sep) at positive ϵ. Spin-selective read out happens at the measurement point (M, white dot). (c) Stability diagram of the transition of interest. The effective hole number is reported as "(n_L, n_R)." The detuning axis as well as I, M, and Sep are highlighted. The dashed triangle marks the PSB region. (d)–(f) Reflection phase versus ϵ and magnetic field for $\theta = 90°$, 60°, and 10°, respectively. A high signal corresponds to a larger triplet return probability. The lower inset in (d) displays the pulse sequence where only the pulse amplitude ϵ is varied.

sensitive to differences in, or the average of, the Zeeman energies of the dots, and hence we define $g^{\pm} = g^L \pm g^R$ as the g-factor difference and sum. The energy spectrum of the system (the complete Hamiltonian H_{tot} is derived in the Supplemental Material [17] Sec. VI) is depicted in Fig. 1(b) as a function of ϵ. At $\epsilon = \epsilon^*$ the S and T_- states anticross.

We start by mapping out Δ_{ST_-} as a function of magnetic field angle by varying the magnetic field strength B and ϵ [24]. We initialize the system deep in (2,0) in a singlet state [point I in Fig. 1(c)], then pulse quickly to (1,1) where the spins are separated (Sep). Mixing between S and T_- is induced when $\epsilon \approx \epsilon^*$. In the end we measure the spin state inside the PSB triangle (M). The resulting triplet return probability depends both on the size of the avoided crossing and the separation time τ_S. We apply a rapid pulse of duration $\tau_S = 65$ ns and varying ϵ [inset of Fig. 1(d)]. Figures 1(d),1(e), and 1(f) depict the phase response of the charge sensor in the measurement point as a function of ϵ and B for $\theta = 90°$, 60°, and 10°, respectively. A high phase signal corresponds to a larger triplet return probability. In the out-of-plane direction we observe the expected funnel shape of the $S - T_-$ anticrossing [24]. At 60° we similarly observe a typical funnel shape, however, we notice the line to be fainter, which indicates a smaller Δ_{ST_-}. The picture drastically changes towards the in-plane direction where the $S - T_-$ avoided crossing develops interference fringes with a pattern resembling a butterfly; 2 components can be attributed to $S - T_-$ oscillations at low detuning and $S - T_0$ oscillations becoming more prominent at high detuning. The angular anisotropy of the funnel pattern, further exemplified in the Supplemental Material [17], Fig. S5, is the main focus of this work and requires knowledge of the full Hamiltonian and therefore an understanding of the interplay between the g-factor anisotropy and the spin-flip element t_{SO}.

In order to extract the g-factor anisotropy we rely on singlet-triplet oscillations. After initialization in $S(2,0)$, appropriate pulses to (1,1) induce either $S - T_0$ or $S - T_-$ oscillations. The probability to maintain the initial eigenstate of the system after a sweep with ramp time τ_R is given by the Landau-Zener formula $P_{\mathrm{LZ}} = \exp[-(2\pi\Delta_{ST_-}^2/\hbar v)]$ [25,26], where $\hbar$ is the reduced Planck constant, $v = |dE/dt| = |dJ(\epsilon)/d\epsilon|_{\epsilon=\epsilon^*}(\Delta\epsilon/\tau_R)$ is the velocity calculated at $\epsilon = \epsilon^*$ and $J(\epsilon) = \sqrt{(\epsilon^2/4) + 2t_C^2} - (\epsilon/2)$ is the exchange energy [Fig. 1(b)] [15]. If v satisfies the diabatic condition ($P_{\mathrm{LZ}} \approx 1$) $S - T_0$ oscillations with a frequency $f = (1/h)\sqrt{J^2 + (g^-\mu_B B)^2}$ will be favored. With $P_{\mathrm{LZ}} < 1$ the $S - T_0$ oscillations are suppressed and the qubit is initialized in a superposition of S and T_-. After a time τ_S the system is pulsed back to the measurement point where another nondiabatic passage will cause an interference between the two states [27]. The accumulated phase difference is then given by $\phi = 2\pi f_{S-T_-}\tau_S \approx (\tau_S/\hbar)|J - \frac{1}{2}g^+\mu_B B|$ [28] [Fig. 1(b)]. As the oscillation frequency of the $S - T_0$ ($S - T_-$) qubit depends on g^- (g^+) [Fig. 1(b)] we can extract the individual g factors without the need for EDSR. We fix the magnetic field at $|B| = 2$ mT and observe the oscillations vs τ_S while rotating B. We use a fast pulse ($\tau_R = \tau_{\mathrm{rise}} = 2$ ns) in Fig. 2(a) and a ramped pulse with ramp time $\tau_R = 100$ ns in Fig. 2(c). In both cases we pulse to $\epsilon = 4$ meV for a duration τ_S. From the fast Fourier transform (FFT) in Figs. 2(b) and 2(d) we extract the oscillation frequency f_{S-T_0} (orange dots) and f_{S-T_-} (pink dots). We notice that for $\theta \in [-25°, +25°]$ in both FFT plots the $S - T_-$ frequency is visible, suggesting that a large coupling term inducing $S - T_-$ oscillations is present at these magnetic field directions, in line with the observations in Fig. 1(f). Moreover, in Fig. 2(d) the FFT power vanishes for $\theta \approx 60°$ indicating that the ramp time τ_R induces a completely diabatic passage over the avoided crossing. This is in line with Fig. 1(e) where we observed a

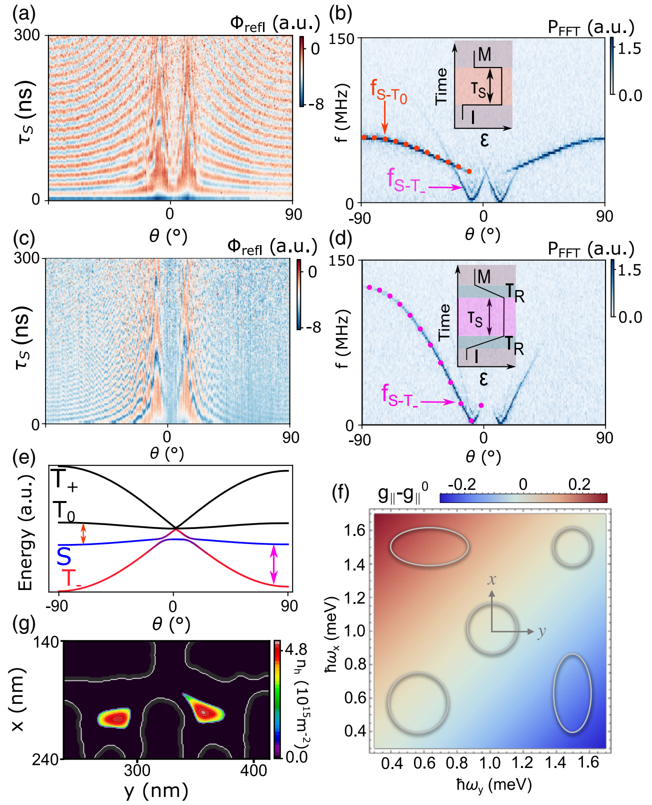

FIG. 2. (a) and (c) Oscillation amplitude of the singlet state in the measurement point as a function of separation time and magnetic field angle at $B = 2$ mT for $\tau_R = 2$ and $\tau_R = 100$ ns, respectively. (b) and (d) FFT of (a) and (c) revealing the oscillation frequency anisotropy. The orange and pink dotted lines are fit to our model. We find a small offset of 100 μT in the perpendicular field which leads to a small asymmetry in the FFT plots. The insets show the pulse shape where the system is swept to $\epsilon = 4$ meV. (e) The energy dispersion of the eigenstates of H_{tot} at $\epsilon = 4$ meV as a function of θ reproduce the frequencies seen in (b),(d) with the orange (pink) arrow highlighting the visible transition. (f) Effect of the confinement on the in-plane g factors for a quantum well width of 20 nm according to Eq. (1). On top, we schematically show possible dot geometries in real space. (g) DQD potential obtained with an electrostatic simulation analogous to that presented in Ref. [29]. Using the gate voltages from the experiment we can infer the approximate dot shapes which shows an almost opposite elongation for the two QDs. The color scale represents the hole density (n_h).

sharper $S - T_-$ avoided-crossing characteristic of a smaller mixing term.

The lines arising in the FFT plots can be fit by the energy splitting between the three lowest lying states of the system depicted in Fig. 2(e) with $g_\perp^+ = 12.00$, $g_\perp^- = 2.04$, $g_\parallel^+ = 0.10$, $g_\parallel^- = 0.43$, and $t_C = 11.38$ μeV. The latter is extracted from exchange oscillation measurements (see Supplemental Material [17] Fig. S2).

Interestingly $|g_\parallel^-| > |g_\parallel^+|$ while $|g_\perp^-| < |g_\perp^+|$. This means that the g factors in the out-of-plane direction have the same sign while they exhibit opposite signs in the in-plane direction. To understand this observation we investigate the effect of the dot geometry on the g factors. As is shown in Supplemental Material [17] Sec. VIII by using the semimicroscopic Luttinger-Kohn Hamiltonian as a starting point, the effects of the intrinsic HH-LH mixing and an elliptical confinement potential can combine to yield g-factor renormalizations. While the correction to the out-of-plane g factor is $|\delta g_\perp| < 10^{-2}$ for the values considered and hence negligible, the in-plane g factor can be altered considerably,

$$g_\parallel = g_\parallel^0 - \xi_1 \frac{\hbar(\omega_x - \omega_y)}{\hbar(\omega_x + \omega_y) - \xi_2 \Delta}. \tag{1}$$

Here, $\xi_1 \approx 20.3$ and $\xi_2 \approx 6.0$ are material specific constants, Δ is the HH-LH splitting, $\hbar\omega_{x,y}$ are the in-plane confinement energies, and $g_\parallel^0 = 0.2$ for Ge [30]. It can be seen from Fig. 2(f) that the in-plane g-factor corrections can be negative in one dot but not in the other for opposite elliptical confinement.

Electrostatic simulations of the DQD potentials arising from the applied gate voltages [29], not accounting for random disorder potentials, confirm the differently shaped dots. In fact, both dots appear elongated with the major axis of the dots being almost perpendicular to each other [Fig. 2(g) shows the calculated hole density n_h and Supplemental Material [17] Sec. IX gives details about the simulation].

We now turn to extract t_{SO} by analyzing Δ_{ST_-} in more detail. We perform Landau-Zener sweeps at $|B| = 20$ mT and extract Δ_{ST_-} from P_{LZ} [Fig. 3(b)] and repeat this for different θ. We vary τ_R during the first passage over the avoided crossing, creating a superposition of S and T_-, and keep the return sweep diabatic in order to maintain this superposition [Fig. 3(a) and inset of Fig. 3(b)]. The extracted Δ_{ST_-} is reported for different θ in Fig. 3(c). In general, Δ_{ST_-} may depend on effects influencing the hole spins such as the g-factor differences in the two dots, the SOI and possible effective magnetic field gradients caused by the hyperfine interaction [31]. While the hyperfine interaction can result in a strong out-of-plane hyperfine component δb_Z for HH states due to a special Ising-type form [32], the inhomogeneous dephasing times extracted for $B_\perp$ of $\approx$700 ns at 1 mT in Ref. [15] give an upper limit for the hyperfine component $\delta b_Z < 2$ neV, suggesting that the effects of the nuclear spin bath may safely be neglected.

In planar HH DQD systems the SOI can be parametrized by a real in-plane spin-orbit vector $\mathbf{t}_{\mathrm{SO}} = (t_x, t_y, 0)$. Such in-plane spin-flip tunneling terms stem from the cubic Rashba SOI [33], while this type of SOI does not induce out-of-plane terms t_z. In a basis in which the total Hamiltonian is diagonal in the absence of the SOI and g-factor differences, the $S - T_-$ splitting has the form [34]

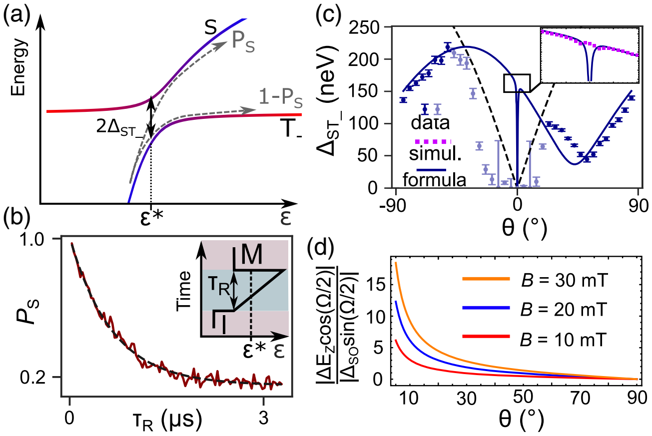

FIG. 3. (a) Energy level diagram of the states involved in the passage over the avoided crossing [red circle in 1(b)]. The probability P_S to maintain a singlet after a single passage over the avoided crossing is given by the Landau-Zener formula. (b) The single LZ passage pulse sequence (inset) leads to a singlet return probability P_S that decays exponentially with the ramp time τ_R. A fit to the Landau-Zener transition formula (black dashed line) allows to extract Δ_{ST_-}. (c) Δ_{ST_-} as a function of magnetic field angle. The extracted Δ_{ST_-} is fit to Eq. (2) with t_x and t_y as fitting parameters (solid blue line). The black dashed line represents the maximum Δ_{ST_-} as a function of θ that can be reliably measured by a single LZ passage. The light colored data points are, therefore, excluded from the fit. (inset) Comparison between the analytical result [solid line, Eq. (2)] and numerical simulation (squares) for Δ_{ST-} around $\theta = 0$. Here, the analytical expression fails due to the small in-plane Zeeman energies. (d) Comparison between the two contributions to Δ_{ST_-}.

$$\Delta_{ST_-} = \left|\Delta_{\mathrm{SO}} \sin\left(\frac{\Omega}{2}\right) + \Delta E_Z \cos\left(\frac{\Omega}{2}\right)\right|, \tag{2}$$

where the spin-orbit splitting Δ_{SO} and the Zeeman splitting ΔE_Z due to anisotropic site-dependent g tensors read

$$\Delta_{\mathrm{SO}} = t_y + it_x \frac{g_\perp^+ \sin\theta}{\sqrt{(g_\parallel^+ \cos\theta)^2 + (g_\perp^+ \sin\theta)^2}}, \tag{3}$$

$$\Delta E_Z = \frac{\mu_B B}{4\sqrt{2}} \frac{(g_\parallel^- g_\perp^+ - g_\parallel^+ g_\perp^-)\sin(2\theta)}{\sqrt{(g_\parallel^+ \cos\theta)^2 + (g_\perp^+ \sin\theta)^2}}, \tag{4}$$

and $\Omega = \arctan(2\sqrt{2}t_C/\epsilon^*)$ is the mixing angle at the anticrossing. The analytical result (2) agrees well with the numerical results obtained by exact diagonalization of the system Hamiltonian for all θ except in a narrow region around $\theta = 0$ [$|\theta| \lesssim 2°$, inset of Fig. 3(c)]. We attribute these deviations to the small in-plane Zeeman energies which violate the assumption of an isolated two-level system made when deriving (2) (see Supplemental Material [17] Sec. VI). Because of the opposite sign g-factor corrections in the dots the Zeeman splitting ΔE_Z can be the dominant contribution to Δ_{ST_-}, exceeding the spin-orbit splitting by one order of magnitude at small angles. Even when the magnetic field has a large out-of-plane component, the effect of different g factors can contribute crucially to Δ_{ST_-} [Fig. 3(d)].

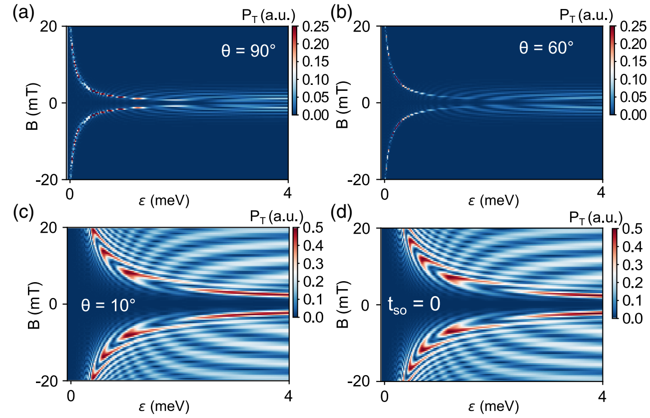

FIG. 4. Simulations of the funnel plots with the master equation approach using qutip. (a)–(c) Funnel for $\theta = 90°$, 60°, and 10°, respectively, showing the $S - T_-$ avoided crossing as an increased triplet return probability. The simulations take the model Hamiltonian with the experimentally extracted parameters as input and perform the time-evolution calculation returning the combined triplet return probability ($P_{T_+} + P_{T_-} + P_{T_0}$). The simulations reproduce the experimental data observed in Fig. 1. (d) A simulation with $t_{\mathrm{SO}} = 0$ but with all the other values of the model as in (c) again reveals the butterfly shape of the $S - T_-$ avoided crossing.

The extracted Δ_{ST_-} in Fig. 3(c) can be fit by the model with t_x and t_y as free parameters and t_C, $g_\perp^+$, $g_\perp^-$, $g_\parallel^+$, $g_\parallel^-$ extracted from previous measurements. Between $-25°$ and $25°$ the splitting seems to drop to zero as the Landau-Zener assumptions of diabatic return sweeps are not met and an extraction of Δ_{ST_-} is not accurate. The black dashed line corresponds to the maximum Δ_{ST_-} that allows a diabatic passage with a rise time of 2 ns of our pulses ($P_{\mathrm{LZ,max}} = 0.99 = \exp[-(2\pi\Delta^2_{\mathrm{ST,max}}/\hbar v)]$). The model fits the dark blue data points with $t_x = 129.0 \pm 18.0$ and $t_y = -369.8 \pm 13.8$ neV, yielding the total spin-flip tunneling element $t_{\mathrm{SO}} = \sqrt{t_x^2 + t_y^2} = 392.0$ neV.

Having characterized all the elements in the Hamiltonian from independent measurements we can now reproduce the funnel measurements in Fig. 1 (Fig. 4). In particular the sharper line at $\theta = 60°$ [Fig. 4(b)] as well as the $S - T_-$ oscillations for $\theta = 10°$ [Fig. 4(c)] reflect what we observe in the data. Even with $t_{\mathrm{SO}} = 0$ the in-plane g-factor difference induces $S - T_-$ oscillations [Fig. 4(d)] further confirming its dominant role in determining the size of Δ_{ST_-}.

In conclusion, we have demonstrated that the g-tensor anisotropy and, in particular, the in-plane g-factor difference can lead to a considerable contribution to Δ_{ST_-} in the in-plane direction. However, Landau-Zener sweeps and singlet-triplet oscillations measured in different magnetic field directions allowed us to distinguish the Zeeman induced coupling from the spin-orbit induced coupling and, thereby, infer the magnitude and orientation of t_{SO}. We reconstructed the experimental data in our simulations confirming the validity of our theoretical model. This understanding of the interplay between t_{SO} and the in plane g-factor difference opens the possibility to operate hole singlet-triplet qubits at sweet spots, for example with orthogonal axis [34]. Our work, therefore, provides important insight into the spin-orbit interaction of hole spin double quantum dot devices and lays the foundation for the design of future hole spin qubit experiments.

This research was supported by the Scientific Service Units of ISTA through resources provided by the MIBA Machine Shop and the nanofabrication facility. This project has received funding from the European Union's Horizon 2020 research and innovation program under the Marie Skłodowska-Curie Grant Agreement No. 844511, No. 75441, and by the FWF-P 30207, I05060, and M 3032-N projects. A. B. acknowledges support from the EU Horizon-2020 FET project microSPIRE, ID: 766955. P. M. M. and G. B. acknowledge funding by the Deutsche Forschungsgemeinschaft (DFG—German Research Foundation) under Project No. 450396347. This work was supported by the Royal Society (URF\R1\191150) and the European Research Council (Grant Agreement No. 948932), N. A. acknowledges the use of the University of Oxford Advanced Research Computing (ARC) facility.

*daniel.jirovec@ista.ac.at
†philipp.mutter@uni-konstanz.de

[1] V. N. Golovach, M. Borhani, and D. Loss, Electric-dipole-induced spin resonance in quantum dots, Phys. Rev. B **74**, 165319 (2006).
[2] D. V. Bulaev and D. Loss, Electric Dipole Spin Resonance for Heavy Holes in Quantum Dots, Phys. Rev. Lett. **98**, 097202 (2007).
[3] X. Wu *et al.*, Two-axis control of a singlet-triplet qubit with an integrated micromagnet, Proc. Natl. Acad. Sci. U.S.A. **111**, 11938 (2014).
[4] J. Yoneda *et al.*, A quantum-dot spin qubit with coherence limited by charge noise and fidelity higher than 99.9%, Nat. Nanotechnol. **13**, 102 (2018).
[5] R. Maurand *et al.*, A CMOS silicon spin qubit, Nat. Commun. **7**, 13575 (2016).
[6] A. Crippa *et al.*, Electrical Spin Driving by g -Matrix Modulation in Spin-Orbit Qubits, Phys. Rev. Lett. **120**, 137702 (2018).
[7] H. Watzinger, J. Kukučka, L. Vukušić, F. Gao, T. Wang, F. Schäffler, J.-J. Zhang, and G. Katsaros, A germanium hole spin qubit, Nat. Commun. **9**, 3902 (2018).
[8] N. W. Hendrickx, W. I. L. Lawrie, L. Petit, A. Sammak, G. Scappucci, and M. Veldhorst, A single-hole spin qubit, Nat. Commun. **11**, 3478 (2020).
[9] N. W. Hendrickx, D. P. Franke, A. Sammak, G. Scappucci, and M. Veldhorst, Fast two-qubit logic with holes in germanium, Nature (London) **577**, 487 (2020).
[10] F. N. M. Froning, L. C. Camenzind, O. A. H. van der Molen, A. Li, E. P. A. M. Bakkers, D. M. Zumbühl, and F. R. Braakman, Ultrafast hole spin qubit with gate-tunable spin–orbit switch functionality, Nat. Nanotechnol. **16**, 308 (2021).
[11] K. Wang *et al.*, Ultrafast operations of a hole spin qubit in ge quantum dot, Nat. Commun. **13**, 206 (2022).
[12] R. Moriya *et al.*, Cubic Rashba Spin-Orbit Interaction of a Two-Dimensional Hole Gas in a Strained-ge/SiGeQuantum Well, Phys. Rev. Lett. **113**, 086601 (2014).
[13] S. Bosco, M. Benito, C. Adelsberger, and D. Loss, Squeezed hole spin qubits in ge quantum dots with ultrafast gates at low power, Phys. Rev. B **104**, 115425 (2021).
[14] Z. Wang, E. Marcellina, A. R. Hamilton, J. H. Cullen, S. Rogge, J. Salfi, and D. Culcer, Optimal operation points for ultrafast, highly coherent ge hole spin-orbit qubits, npj Quantum Inf. **7**, 54 (2021).
[15] D. Jirovec *et al.*, A singlet-triplet hole spin qubit in planar Ge, Nat. Mater. **20**, 1106 (2021).
[16] R. J. Schoelkopf, P. Wahlgren, A. A. Kozhevnikov, P. Delsing, and D. E. Prober, The radio-frequency single-electron transistor (RF-SET): A fast and ultrasensitive electrometer, Science **280**, 1238 (1998).
[17] See Supplemental Material at http://link.aps.org/supplemental/10.1103/PhysRevLett.128.126803 for pulse calibrations, additional data and details of the theoretical model derivation, which includes Ref. [18–23].
[18] X. Marie, T. Amand, P. Le Jeune, M. Paillard, P. Renucci, L. E. Golub, V. D. Dymnikov, and E. L. Ivchenko, Hole spin quantum beats in quantum-well structures, Phys. Rev. B **60**, 5811 (1999).
[19] A. V. Trifonov *et al.*, Strong enhancement of heavy-hole landé factor q in ingaas symmetric quantum dots revealed by coherent optical spectroscopy, arXiv:2103.13653.
[20] G. Granger, G. C. Aers, S. A. Studenikin, A. Kam, P. Zawadzki, Z. R. Wasilewski, and A. S. Sachrajda, Visibility study of $\mathrm{S}-\mathrm{T}_+$ landau-zener-stückelberg oscillations without applied initialization, Phys. Rev. B **91**, 115309 (2015).
[21] L. A. Orona, J. M. Nichol, S. P. Harvey, C. G. L. Bøttcher, S. Fallahi, G. C. Gardner, M. J. Manfra, and A. Yacoby, Readout of singlet-triplet qubits at large magnetic field gradients, Phys. Rev. B **98**, 125404 (2018).
[22] J. Danon and Y. V. Nazarov, Pauli spin blockade in the presence of strong spin-orbit coupling, Phys. Rev. B **80**, 041301(R) (2009).
[23] V. N. Golovach, A. Khaetskii, and D. Loss, Phonon-Induced Decay of the Electron Spin in Quantum Dots, Phys. Rev. Lett. **93**, 016601 (2004).
[24] J. R. Petta, Coherent manipulation of coupled electron spins in semiconductor quantum dots, Science **309**, 2180 (2005).
[25] L. D. Landau, Zur theorie der energieübertragung. II., Phys. Sov. Union **2**, 46 (1932).
[26] C. Zener, Non-adiabatic crossing of energy levels, Proc. R. Soc. A **137**, 696 (1932).

[27] S. Shevchenko, S. Ashhab, and F. Nori, Landau–zener–stückelberg interferometry, Phys. Rep. **492**, 1 (2010).

[28] J. R. Petta, H. Lu, and A. C. Gossard, A coherent beam splitter for electronic spin states, Science **327**, 669 (2010).

[29] D. L. Craig *et al.*, Bridging the reality gap in quantum devices with physics-aware machine learning, arXiv:2111.11285.

[30] R. Winkler, *Spin—Orbit Coupling Effects in Two-Dimensional Electron and Hole Systems* (Springer, Berlin, Heidelberg, 2003).

[31] D. Stepanenko, M. Rudner, B. I. Halperin, and D. Loss, Singlet-triplet splitting in double quantum dots due to spin-orbit and hyperfine interactions, Phys. Rev. B **85**, 075416 (2012).

[32] J. Fischer, W. A. Coish, D. V. Bulaev, and D. Loss, Spin decoherence of a heavy hole coupled to nuclear spins in a quantum dot, Phys. Rev. B **78**, 155329 (2008).

[33] P. M. Mutter and G. Burkard, Natural heavy-hole flopping mode qubit in germanium, Phys. Rev. Research **3**, 013194 (2021).

[34] P. M. Mutter and G. Burkard, All-electrical control of hole singlet-triplet spin qubits at low-leakage points, Phys. Rev. B **104**, 195421 (2021).